International Journal of Greenhouse Gas Control 87 (2019) 44–57

Contents lists available at ScienceDirect

International Journal of Greenhouse Gas Control

journal homepage: www.elsevier.com/locate/ijggc

Modeling and simulation of the start-up process of coal fired power plants with post-combustion CO_2 capture

Thomas Marx-Schubach*, Gerhard Schmitz

Institute of Engineering Thermodynamics, Hamburg University of Technology, Denickestrasse 15, 21073 Hamburg, country

ARTICLE INFO

Keywords:
Post-combustion capture
CCS
Start-up
Modeling
Coal-fired power plant
Dynamic simulation

ABSTRACT

A detailed model of a post-combustion CO_2 capture plant (pcc-plant) is developed in the Modelica® language which allows the simulation of start-up and shutdown processes. The model of the pcc-plant is coupled to a simplified model of a coal fired power plant to investigate the coupled process. To guarantee a stable and automatic operation, a sequential control for start-up and shutdown procedures is implemented in both plants. Two case studies, focussing on the pcc-plant, are subsequently performed in this contribution. In the first case study, the influence of different parameters and input variables on the start-up time is investigated in order to analyze the start-up process of the pcc-plant. The varied variables are the steam flow rate to the reboiler, the solvent flow rate and the total amount of solvent in the pcc-plant. In the second case study two different start-up control structures for the carbon capture plant are proposed and their performances are presented and compared.

1. Introduction

At the United Nations Climate Change Conference (COP 21) in 2015, 196 countries accepted the Paris agreement to reduce their carbon emissions. The common goal is to keep the global warming "well below" 2 °C. The carbon capture and storage technology (CCS) is one opportunity to capture CO_2 emissions from flue gases of combustions processes. One possible application is the capturing of CO_2 from flue gases of thermal power plants. The captured CO_2 can be stored in underground formations afterwards.

In general, several technologies for capturing the CO_2 can be used. One possibility is the post-combustion capture (pcc) technology in which the CO_2 is captured without changing the combustion process. The main advantage is that the influence on the combustion process and the power plant is relatively low compared to the pre-combustion and oxyfuel technologies. The technology is also the most mature (Bhown and Freeman, 2011) and existing power plants can be retrofitted with this technology (Garðarsdóttir et al., 2017). In the oxyfuel technology, the fuel is burned in the combustion chamber of the power plant using pure oxygen which results in a flue gas consisting of H_2O and CO_2 only. In the pre-combustion technology, the coal is gasified and reformed. Subsequently, the CO_2 is separated from the hydrogen resulting in a synthesis gas that can be burned in a gas turbine for example.

Even if the share of renewable energies increases nowadays, fossil power plants will still play a key role in the future until a sufficient infrastructure of suitable energy storage systems will be developed and built or other solutions will be found. In order to balance the frequency change in the power grid, fossil power plants have to be operated in a very flexible way. This implies that load changes, start-up and shutdown sequences will occur more frequently in the future (Lew et al., 2012). Therefore, a lot of research projects are carried out in this field of study, aiming at faster and more cost-effective load changes as well as start-up and shutdown procedures (Montanés et al., 2018). Many publications deal with the investigation of the dynamic behavior of carbon capture processes using dynamic models (Bui et al., 2014). These models are often used to develop suitable control structures and to investigate their capability of balancing disturbances (Panahi and Skogestad, 2012; Nittaya et al., 2014; Montanés et al., 2017; Luu et al., 2015; Mechleri et al., 2017; Lin et al., 2012; Sepideh Ziaii Fashami, 2012) which is indispensable for a safe and flexible operation of the plant. Besides conventional control systems using PID controllers also more sophisticated control systems such as model predictive control are developed (Åkesson et al., 2012; Wu et al., 2018; Zhang et al., 2016).

Although a large amount of literature deals with thermal separation processes in general, only few publications address the modeling and simulation of the start-up of thermal separation processes in general or the pcc-process in particular. Kvamsdal et al. (2009) and Jayarathna et al. (2013) developed a non-equilibrium model for the start-up of an

* Corresponding author.
E-mail addresses: thomas.marx@tuhh.de (T. Marx-Schubach), schmitz@tuhh.de (G. Schmitz).

https://doi.org/10.1016/j.ijggc.2019.05.003
Received 2 October 2018; Received in revised form 18 April 2019; Accepted 3 May 2019

Nomenclature

Abbreviations

CCS	carbon capture and storage
DAE	differential algebraic equation
DOF	degree of freedom
HP	high pressure
IP	intermediate pressure
L/G ratio	liquid to gas ratio
LP	low pressure
MEA	monoethanolamine
MPC	model predictive control
PCC	post-combustion carbon capture

Greek symbols

α	solvent loading in mol_{CO_2}/mol_{MEA} or heat transfer coefficient in $W/(m^2\,K)$
η	efficiency
λ	thermal conductivity in W/(m K)
ρ	density in kg/m^3
σ	Stefan–Boltzmann constant in $W/(m^2\,K^4)$
ε	emissivity

Latin symbols

A	area in m^2
a	weighting factors for calculation of radiation
A_s	absorbance of suspension m^2
c	molar concentration in mol/m^3
$CF_{fouling}$	calibration factor for fouling
$\dot{H}$	enthalpy flow in J/s
h	specific enthalpy in J/kg
k	mass flow ratio
K	calibration factor for approximate equilibrium condition
$\dot{m}$	mass flow rate in kg/s
m	mass in kg
$\dot{N}$	molar flow rate in mol/s
P	power in W
p	pressure in bar or Pa
$\dot{Q}$	heat flow rate in W
Q	amount of heat in J
T	temperature in °C or K
t	time in s
$\dot{V}$	volume flow rate in m^3/s
w	particle velocity in m/s
X	CO_2 capture rate
y	vapor mole fraction

Subscripts

*	composition at phase boundary
bub	bubble
conv	convection
g	gas
i	component or sums
is	isentropic
j	index for stage or volume
L	solvent
lean	CO_2 lean condition
liq	liquid
mech	mechanical
opt	optimal
rad	radiation
reb	reboiler
rich	CO_2 rich condition
s	suspension
st.	steam
str	stripper
sys	system
trans	mass transfer
vap	vapor
w	wall

absorption unit of an amine based pcc-plant. Gaspar et al. (2015) also presented a model for the simulation of the start-up process of a pcc-plant. The heating-up process in the stripper is neglected and not simulated in these publications. They use a storage tank filled with regenerated solvent to start the solvent flow to the absorber.

Wellner (2016) developed a start-up model of the entire pcc-plant which covers also the heating-up process in the stripper. This model is used in this contribution to describe the start-up process of the pcc-plant in an extended form.

Several publications also investigate the coupled process of coal fired power plants combined with post-combustion capture. The goal is to study the combined process in detail and to investigate the impact of the pcc-plant on the power plant. They often conclude that the dynamics of the power plant are much faster than the dynamics of the pcc-plant (Lawal et al., 2012). Wellner et al. (2016) successfully proved the technical possibility of providing primary frequency control by throttling the reboiler steam valve, using dynamic simulations of the combined process. In the scenario, the power output of the power plant is controlled using feed forward control.

Garðarsdóttir et al. (2017) used different PID control systems in a likewise scenario, concluding that the generator power in the combined system cannot be stabilized by the control system when the reboiler valve is throttled. They recommend to test advanced control systems in the future to improve settling times. Montanés et al. (2017b) analyzed the load change dynamics of a natural gas power plant coupled with a pcc-process. The authors pointed out that the coupled power plant is still able to follow common load changes in operation when an appropriate control scheme is used.

Walters et al. (2016) developed a steady state model of a power plant combined with a dynamic pcc-model. The model is used to gain more knowledge about the process, resulting in different recommended control strategies in combined operation. Zhang et al. (2016) modeled a 550 MW supercritical power plant integrated with a pcc-unit and compare the performance of a PID control scheme and a MPC in combined operation. Dutta et al. (2017) designed two different absorber configurations for a 600 MW natural gas fueled power plant and tested their operability with dynamic simulations.

Mac Dowell and Shah (2014, 2015) use a dynamic model of a subcritical power plant with a pcc-plant to study the profitability of different process scenarios during flexible operation of the combined plant including flue gas bypass, time-varying solvent regeneration and solvent storage. They concluded that the time-varying solvent regeneration scenario leads to the highest increase of profitability (Mac Dowell and Shah, 2015). However, all these publications deal with the regular operation of the plant. They do not simulate the start-up and shutdown of the combined process. To close this gap, a detailed model of a post-combustion capture plant is developed in this publication, which allows the simulation of the start-up and shutdown process. Subsequently, the model is coupled to a simplified model of a coal fired power plant to study the combined process.

In the following section, the pcc-process and the power plant process are described briefly. Afterwards, the model and the development of the sequential control schemes are presented. The model is developed using the open-source modeling language Modelica® (Modelica Association, 2017). The simulations are carried out in the simulation environment Dymola® by Dassault Systèmes. For the simulation of the pcc-process the *ThermalSeparation* library is used (Joos et al., 2009; Dietl, 2012). The model was validated with pilot plant data of a pcc-plant located in Heilbronn, Germany (Rieder and Unterberger, 2013; Mejdell et al., 2017) which has been already done in earlier publications (Wellner, 2016; Marx-Schubach and Schmitz, 2017). The model of the power plant is developed using the *ClaRa* library (ClaRa-Library, 2019; Gottelt et al., 2017) in cooperation with the Institute of Energy Systems at the Hamburg University of Technology.

Subsequently, the sequence control systems are presented. The sequence control of the power plant is taken from the power plant located in Heyden, Germany, and implemented into the model in a simplified form. The sequence control model for the pcc-plant is developed in this publication. The resulting model is used to simulate different case studies with focus on the pcc-plant. First, the most important input variables (steam flow rate to reboiler and solvent flow rate) are varied to investigate their influence on the start-up process. Furthermore, the total amount of solvent in the pcc-plant is varied. In the second step, two different sequential control structures are tested and compared.

2. Process description

In this section, the power plant and pcc-process are described briefly. For the realization of the pcc-process, an aqueous amine scrubbing process using columns with structured packings is chosen as it is supposed to be the most mature process (Leung et al., 2014; Rochelle, 2009). More detailed information about the coupling between both processes can be found in Wellner et al. (2016).

2.1. Power plant process

In Fig. 1 a simplified flow scheme of the water steam cycle of a power plant is illustrated. In the steam generator, the water is evaporated and superheated. The steam is then expanded in the high pressure turbine (HP turbine). After the intermediate superheating, the steam is expanded in the intermediate (IP) and low pressure turbine (LP turbine). The process steam for the pcc-plant is typically extracted between the IP and LP turbine. Afterwards, the steam is fully condensed in the condenser and pumped through the low pressure preheater to the feed water tank where part of the feed water is stored. The feed water is preheated in the HP preheating unit and flows back to the steam generator.

2.2. Post-combustion capture process

The pcc-process in this publication is a conventional amine based scrubbing process. The solvent is an aqueous monoethanolamine (MEA) solution with 30 wt% MEA. The main reason for using MEA is that the material data of MEA are well reported in the literature. The plant consists mainly of three columns, which are usually filled with structured or random packings to increase the effective mass transfer area and achieve a high mass transfer rate in the columns.

In Fig. 2 a simplified process flow diagram is depicted. In the first step, the flue gas is washed with diluted aqueous sodium hydroxide solution to wash sulfur dioxide out of the flue gas and is cooled to approximately 35 °C. The flue gas is compressed in a blower afterwards, which can also be situated upstream the flue gas cooler or downstream the absorber. The flue gas is fed into the absorber, which is operated at ambient pressure, and flows upstream through the absorption section where the CO_2 is removed from the flue gas. The washing section at the top of the absorber is used to wash out amine residues from the flue gas. The solvent flows countercurrent to the flue gas and the carbon dioxide is chemically absorbed by the solvent. The rich solvent is collected in the absorption sump from where it is pumped through a heat exchanger to the stripper which operates at a higher pressure of 2 bar and a higher temperature of about 120 °C. Subsequently, the solvent is heated up by the steam flow into the reboiler leading to a desorption of the CO_2 and a regeneration of the solvent. The steam is extracted from the water steam cycle of the power plant, typically between the intermediate and low pressure turbine. After the desorption, most of the remaining steam in the CO_2 flow is condensed in the condenser. Then, the emitted CO_2 can be compressed and stored in underground formations. The regenerated solvent is used to preheat the rich solvent in the central heat exchanger and pumped back to the absorber.

3. Model description

The model is developed using the Modelica® (Modelica Association, 2017) modeling language and the simulations are carried out in the simulation environment Dymola® developed by Dassault Systèmes. The pcc-unit is modeled with the *ThermalSeparation* library (Joos et al., 2009; Dietl, 2012) and the *ClaRa* library was used to model the power plant (ClaRa-Library, 2019; Gottelt et al., 2017). An overview of the developed model can be seen in Fig. 3. The models are described in the following subsections. The section is finished with a description of the developed sequential control structures.

3.1. Modeling the power plant

The modeled power plant is based on the coal fired single block supercritical power plant with a 920 MW gross electric output located in Heyden, Germany. During the modeling process, several simplifications were made to allow for a fast and robust simulation of the combined process. Therefore, the results are not directly related to measurements results. The model can be used to simulate the regular operation of the plant in a load range of 23–100% and the start-up and shutdown of the power plant.

The milling process is not modeled. Therefore, the coal dust is an input variable and is mixed immediately with the primary air in the model and fed to the combustion chamber.

The steam generator of the power plant is a Benson® boiler with two passes. The combustion chamber is fired by 4 burner levels whereas in the model the burner sections are combined to a single burner section. The geometry of the steam generator is adapted to Heyden power plant data. The gas side is modeled using a number of discretized gas volumes with a stationary fuel mass balance in the burner, a dynamic flue gas mass and component balances and a simple energy balance. The water side is modeled using discretized pipes with a static momentum balance

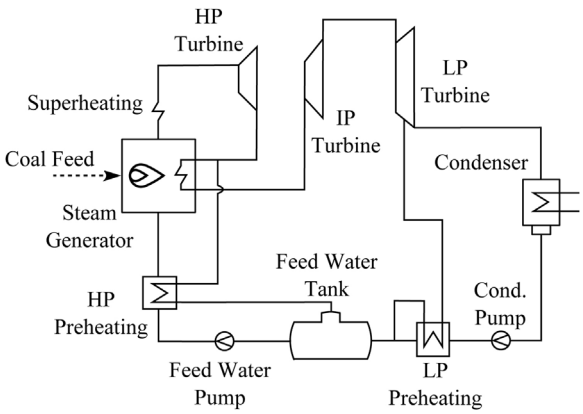

Fig. 1. Simplified process flow diagram of the water steam cycle of a power plant (Wellner et al., 2016).

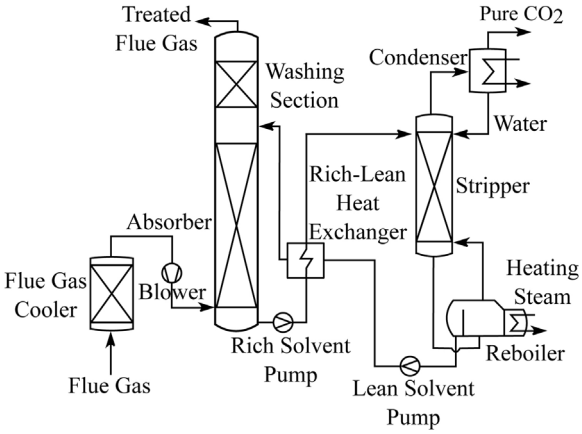

Fig. 2. Simplified process flow diagram of a post-combustion capture plant (Wellner et al., 2016).

and dynamic mass, energy and component balances. The overall mass balance in the pipes is given in the following simple form.

$$\frac{d\rho_j}{dt}\cdot V_j = \dot{m}_j - \dot{m}_{j+1} \tag{1}$$

$\dot{m}_j$ and $\dot{m}_{j+1}$ are the inlet and outlet mass flows of element j and ρ_j is the density in the element j with volume V_j. The energy balance is calculated in the following way, where h_j is the specific enthalpy and p_j the pressure in the pipe section with volume V and $\dot{Q}_{w,j}$ is the heat transferred through the pipe wall.

$$\frac{dh_j}{dt} = (\dot{H}_j - \dot{H}_{j+1} + \dot{Q}_{w,j} + \frac{dp_j}{dt}\cdot V_j - h_j\cdot V_j\cdot\frac{d\rho_j}{dt})\cdot\frac{1}{m_j} \tag{2}$$

$\dot{H}_j$ and $\dot{H}_{j+1}$ are the enthalpy inlet and outlet flows of the section and ρ_j is the density of the fluid in the pipe section. The total mass of fluid in the element is m_j.

The pressure loss in the pipes is calculated using a simple linear pressure drop model. On the water side, a steam water separator is installed between the evaporator and the first superheating unit, which is used in the part load operation of the plant.

The heat transfer to the wall is calculated in all gas volumes in the steam generator using a radiation model from the German reference book VDI Wärmeatlas in chapter K5 (VDI e.V., 2013), in which the radiative heat flow is approximated by a summation formula. Additionally, a fouling factor is introduced to take the fouling of the wall into account. The fouling factors $CF_{fouling}$ are used to adjust the heat transfer according to measurement data.

$$\dot{Q}_{rad,g} = \mathrm{CF}_{fouling}\cdot A_{heat}\cdot\sigma\cdot \sum_{i=1}^{3}\frac{\varepsilon_{s,i}\cdot\varepsilon_w}{1-(1-\varepsilon_w)\cdot(1-\varepsilon_{s,i})}\cdot[a_{i,w}\cdot T_w^4 - a_{i,g}\cdot T_g^4] \tag{3}$$

A_{heat} is the area of the wall, σ is the Stefan-Boltzmann constant, $\varepsilon_{s,i}$ is the suspension emissivity factor, ε_w the emissivity of the wall, which is fixed to $\varepsilon_w = 0.8$. $a_{i,w}$ and $a_{i,g}$ are weighting factors which are dependent of the gas temperature T_g and the wall temperature T_w. The emissivity of the suspension $\varepsilon_{s,i}$ and the weighting factors $a_{i,w}$ and $a_{i,g}$ are also calculated according to the rules in the VDI Wärmeatlas.

The heat transfer on the gas side to the wall of the tube bundles $\dot{Q}_{tb,g}$ in the superheater, reheater and economizer is described using a combined convection ($\dot{Q}_{conv,g}$) and radiation ($\dot{Q}_{rad,g}$) approach.

$$\dot{Q}_{tb,g} = \dot{Q}_{conv,g} + \dot{Q}_{rad,g} \tag{4}$$

The contribution of the radiative heat transfer $\dot{Q}_{rad,g}$ is calculated in the following way (VDI e.V., 2013).

$$\dot{Q}_{rad,g,tb} = \frac{\mathrm{CF}_{fouling}\cdot A_{heat}\cdot\sigma\cdot\varepsilon_{tubes}}{A_s + \varepsilon_{tubes} - A_s\cdot\varepsilon_{tubes}}\cdot[A_{susp}\cdot T_w^4 - \varepsilon_s\cdot T_{mean}^4] \tag{5}$$

ε_{tubes} is the emissivity of the tubes, A_s the absorbance of the suspension and T_{mean} is the mean temperature of the gas in the volume.

The convective heat transfer on the gas side is calculated with the heat transfer coefficient $\alpha_{conv,g}$, the heat transfer area A_{heat} and the temperature difference between the inlet temperature of the fluid $T_{g,in}$

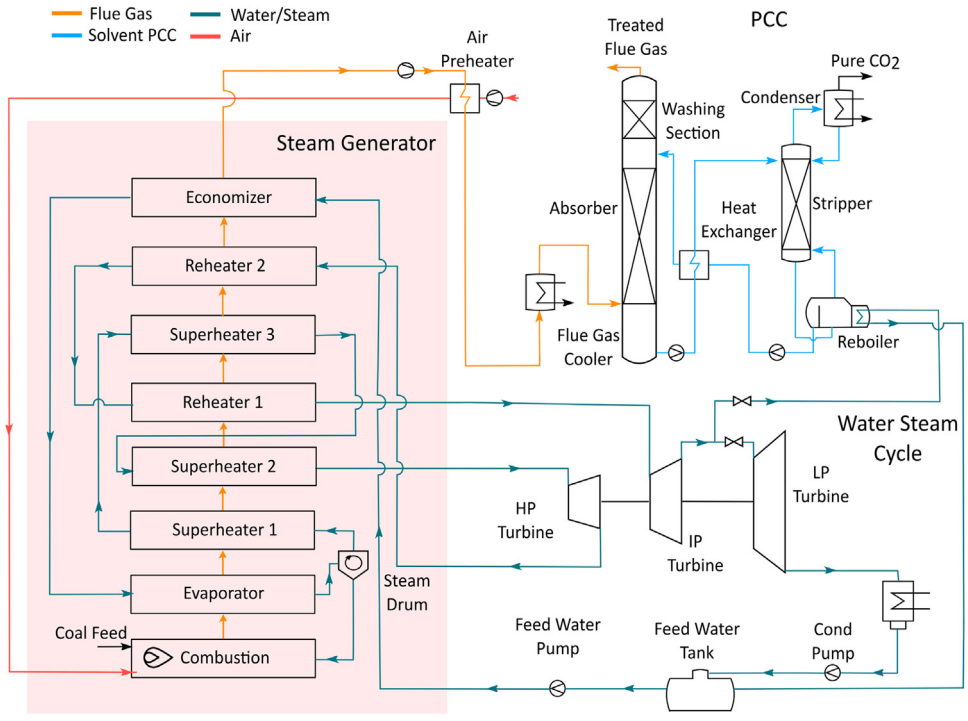

Fig. 3. Model overview of the combined model.

and the tube wall temperature T_{wall}.

$$\dot{Q}_{conv,g} = \alpha_{conv,g} \cdot A_{heat} \cdot (T_{wall} - T_{g,in}) \quad (6)$$

The heat transfer coefficient for the convection is also calculated according to correlations in the VDI Wärmeatlas (VDI e.V., 2013).

The heat transfer on the water side is described using a convection model with a heat transfer coefficient of $\alpha_{conv,liq} = 10,000\ W/(m^2\ K)$ in the evaporator and $\alpha_{conv,liq} = 3000\ W/(m^2\ K)$ in the other sections. A_{heat} is the mean surface of the tubes, T_{wall} is the temperature at the inner tube wall, and $T_{liq,out}$ the temperature of the fluid at volume outlet. A characteristic line is used to take the part load dependency of the heat transfer coefficients into account.

$$\dot{Q}_{conv,liq} = \alpha_{conv,liq} \cdot A_{heat} \cdot (T_{wall} - T_{liq,out}) \quad (7)$$

The burner section is modeled using a gas volume section with a constant burning time of $t = 0.5\ s$. Additionally, a fixed particle migration speed of $w_{fixed} = 1.5\ m/s$ is assumed. With these assumptions, the fuel is burned completely in the burner section.

The evaporator consists of three gas volumes and a discretized pipe with eight finite volumes whereas the second and third superheater, reheater and economizer sections consists each of one gas volume and one pipe representing the tube bundle pipes. In the reference plant, the water walls cover the entire flue gas path. However, in the second part of the flue gas path the working fluid is already superheated slightly in the water walls. In the model, this is declared as the first superheater section, which consists of two additional gas volumes without tube bundles. Therefore, only the radiation heat flow to the wall is considered in the first two elements. Also the radiation to the wall in the upper superheater and reheater gas volumes is taken into account. Each heat flow connector is connected to one finite volume in a discretized pipe model representing the water walls.

The turbine is split in a high, intermediate and low pressure part. The turbines are modeled in a simplified way and steady state. The turbine shaft is not modeled. Therefore, the temperature and heat capacity of the shaft and also the shell of the turbine is neglected. The pressure drop is calculated using Stodola's law (David, 1984) where the pressure drop is a function of the nominal mass flow rate and the nominal pressure at turbine inlet and outlet (Alobaid, 2018). For all turbines, a mechanical efficiency of $\eta_{mech} = 0.98$ is assumed. The isentropic efficiency are considered to be $\eta_{is} = 0.9$ for the high and intermediate turbine and $\eta_{is} = 0.87$ in the low pressure turbine. The enthalpy of the steam at the turbine outlet h_{out} is calculated in the following way where h_{in} is the enthalpy at turbine inlet and h_{is} is the enthalpy at the turbine outlet in case of an isentropic process.

$$h_{out} = \eta_{is} \cdot (h_{is} - h_{in}) + h_{in} \quad (8)$$

In the condenser, the shell side is modeled using a vessel. The condenser temperature is set to 30 °C as a fixed boundary condition. The required cooling load is calculated according to this temperature. The tube side of the condenser is not modeled separately. The fluid in the vessel is in thermodynamic equilibrium and subcooling is not considered. The feed water tank is modeled using a volume element with liquid and vapor phase in equilibrium.

The condenser and feed water pump are also modeled in a simplified way. The volume flow of the pump is calculated from the pressure difference Δp and the drive power P_{drive}.

$$\dot{V} = \frac{P_{drive}}{\Delta p} \quad (9)$$

The high pressure and low pressure preheaters are neglected which leads to a reduction of the plant efficiency but also to a significant reduction of simulation times. This can be explained by the fact that the zero mass flows occurring in the preheaters during downtimes of the plant increase the simulation time as the DAE solver has difficulties to solve the resulting equation system.

The control system and the step sequences for shutdown and start-up of the power plant are implemented from the control system of the Heyden power plant in a simplified form. Until now, the model can only be used to model a hot/warm start-up of the power plant.

3.2. Modeling the pcc-plant

The developed pcc-model capable of simulating the start-up process of the pcc-plant is based on the model developed by Wellner (2016) and was validated with measured data from a pilot plant located in Heilbronn, Germany in a previous publication (Marx-Schubach and Schmitz, 2018; Wellner, 2016).

The underlying basic equations of the columns and auxiliary components can be found in the thesis of Dietl (2012). The model of the pcc-plant for the regular operation of the plant is described in the publication from Wellner et al. (2016).

For the simulation of the start-up and shutdown process of the pcc-plant some changes to the model from Wellner et al. (2016) were made. A first version of this start-up model was also published by Wellner (2016). For the sake of simplification, the flue gas cooler is replaced with a simple heat exchanger with a pressure drop where the flue gas is cooled and the sulfur dioxide is directly removed. The columns are modeled as equilibrium-stage-model where the mass transfer equations are neglected. A calibration factor in the absorber takes the deviation from ideal equilibrium conditions into account. In the stripper, no calibration factor is needed as the mass transfer is much faster due to the higher temperatures.

First of all, for the simulation of the shutdown process the ambient heat loss in the columns can no longer be neglected. Therefore, a heat transfer through the column wall is modeled. On the outside wall, natural convection is assumed and the heat transfer coefficient is calculated using a correlation from the German reference book VDI Wärmeatlas (VDI e.V., 2013). The heat conduction through the wall is taken into account using the thermal conductivity coefficient of the wall material. In the desorption unit the insulation is also taken into account. The considered insulation material is mineral wool with a constant thermal conductivity of $\lambda = 0.04\ W/(m\ K)$ (Szodrai and Lakatos, 2014).

The model of the pcc-plant can be initialized in a cold and off state, but the power plant model can only be initialized in steady state. Therefore, the entire model is always initialized in normal operation at steady state. Afterwards, the plant is shut down and started after a selected downtime.

Except the mentioned calculation of the heat loss, changing the equations in the absorption unit is not necessary, as the boiling point is not reached. The filling process of the column and the beginning flue gas flow can be described by the available equations.

The equations in the stripper are adapted to simulate the start-up process as the heating-up process in the stripper cannot be described by the equations in regular operation. The start-up process of the stripper is divided into different steps. This approach is based on the model of Wang et al. (2003). At the beginning of the start-up process, the temperature of the solvent (aqueous monoethanolamine (MEA)) is below the boiling point. This means that the equilibrium condition between the liquid and vapor phase must not be valid to avoid a mass transfer over the phase boundary. Therefore, the mass flow over the phase boundary must be set to zero in the first step.

$$\dot{N}_{j,i}^{vap,trans} = 0 \quad (10)$$

The pressure p_j^{sys} cannot be calculated by the total amount of substances in the vapor phase and must be set by the user. The initial pressure p_j^{init} is usually the ambient pressure.

$$p_j^{sys} = p_j^{init} \quad (11)$$

In the second step, the boiling point is first reached in the reboiler,

leading to a partial evaporation of the solvent. Therefore, the pressure in the columns increases and corresponds to the vapor pressure that is determined by the total amount of substances p_j^{vap}. The pressure is controlled by a pressure valve downstream the stripper head.

$$p_j^{sys} = p_j^{vap} \tag{12}$$

The evaporated solvent enters the first stage of the stripper. In the model, the vapor phase in the stripper consists of steam and carbon dioxide. MEA is considered to exist in the liquid phase only. At this moment, the boiling point in the stage is not reached yet. It is assumed that the entering steam condenses immediately and the carbon dioxide does not react with the solvent as the solvent is loaded with carbon dioxide.

$$\text{For}CO_2: \quad \dot{N}_{j,i}^{vap,trans} = 0,$$
$$\text{For}H_2O: \quad \dot{N}_{j,i}^{vap,trans} = \dot{V}_{j-1,i}^{vap,in} \cdot c_{j-1,i}^{vap,in} \tag{13}$$

When the boiling point in the stage is reached, which means that the vapor pressure p^{bub} reaches the system pressure p^{sys}, the equilibrium condition should be fulfilled in the third step. The switching to the equation $y_{j,i} = y_{j,i}^*$, where $y_{j,i}$ is the mole fraction of component i in the vapor phase of stage j and $y_{j,i}^*$ is the mole fraction at the phase boundary, appears consistent. However, the resulting equation system cannot be solved by the solver (Dietl, 2012). Therefore, the equation is switched to an “apparent equilibrium”-condition for both vapor components.

$$\dot{N}_{j,i}^{vap,trans} = -K \cdot (y_{j,i} - y_{j,i}^*) \tag{14}$$

The value for the constant K should be chosen as high as possible to achieve only an infinitesimal small difference between the vapor mole fraction in the bulk phase and the vapor mole fraction at the phase boundary. To allow a smooth switching between the equations, a smoothing function for the mass flow over the phase boundary is implemented. The other equations remain the same in the stripper.

For the following case study, the process is scaled up with Aspen Plus® to industrial scale capable of treating the entire flue gas flow of the power plant. This results in three parallel capture plants, as the maximum diameter is limited due to structural limitations[1] (Ramezan et al., 2007; Lawal et al., 2012) and the maximum diameter of the used structured packing Sulzer Mellapak 250Y of 15 m (Sulzer Chemtech, 2018). The diameter was calculated in Aspen Plus® with the “fractional approach to maximum capacity” where the diameter is adjusted in such a way that the column is operated at a defined fraction of the flooding point velocity (Agbonghae et al., 2014). A fraction of 0.7 was chosen according to a recommendation by Kister (1992). The height of the columns was adapted manually to achieve the same plant efficiency as in the pilot plant. For the sake of simplification, only one capture plant is represented in the combined model and the flue gas flow into the absorber and steam flow into the reboiler is divided by three. It is assumed that the parallel capture plants show the same behavior. The details of the column geometry are shown in Table 1. Please note that the diameters of the absorbers are slightly higher than the recommendation of Ramezan et al. (2007), but a smaller diameter would lead to a fourth plant or to lower safety margins concerning flooding of the column.

3.3. Integrating the pcc-plant into the power plant

The pcc-plant and the power plant process have two connection points. First, the flue gas of the power plant is fed to the pcc-plant after the flue gas desulphurization process. Second, process steam is extracted between the intermediate and low pressure turbine. The condensed fluid is normally fed back to the low pressure preheating system in the water steam cycle. As the preheaters are neglected in the model, the water is fed back to the feed water tank. For the pcc-plant the steam quality is of great importance to achieve a continuous desorption process in the stripper. Therefore, the pressure in the reboiler tubes may not fall below a certain value. In this case, a sufficient pressure of 3 bar was chosen as sufficient, which results in a temperature difference of approximately 10 K between the shell and the tube side in the reboiler as proposed from Oexmann (2011). As approximately half of the steam is extracted between the intermediate and low pressure turbine, the pressure between the intermediate and low pressure turbine decreases, especially in part load operation. To avoid that the pressure in the reboiler tubes drops below 3 bar, a pressure maintaining valve is installed before the low pressure turbine.

Table 1
Overview of the column geometry.

	Absorber	Stripper
Quantity	3	3
Diameter	14.51 m	8.51 m
Packing Height	15 m	10 m

3.4. Development of sequential control structures

For a safe and automatic start-up, the development of suitable sequential control structures is crucial. The control system is split up into two areas in the model. PI controllers from the *ClaRa* library are used to control the regular operation of the plant and the start-up is controlled using a step sequence by switching the controllers between manual and automatic operation. The step sequences are implemented in the model using the *Modelica-StateGraph2* library. The sequential control structures should fulfill the following requirements and goals:

- The switching between the steps should be as smooth as possible.
- All measured values should stay inside their desired limits to avoid damage to any components.
- The start-up should work automatically without manual interventions and should also cope with small disturbances.
- The step sequence should guarantee a minimal steam flow to the low pressure turbine as well as into the reboiler.

Considering a nominal flue gas flow rate and process constraints (e. g. level controllers, MEA concentration in the solvent) two unconstrained degrees of freedom (DOF) remain that can be used to operate the pcc-plant in an optimal way (Panahi and Skogestad, 2011). In general, the two remaining DOFs are used to control a temperature on a specific stripper tray or the reboiler temperature and the carbon capture rate (Montanés et al., 2017). In this publication, two common control structures are used in regular operation (Fig. 4 and Fig. 5). In the first control structure (Fig. 4), the solvent flow rate $\dot{V}_L$ of the solvent pump downstream the stripper is used to control the capture rate and the reboiler steam valve (proportional to heat flow $\dot{Q}_{reb}$) is used to control the reboiler temperature T_{reb}. In the second control structure (Fig. 5), the solvent flow rate of the stripper pump controls the stripper temperature on the lowest stripper stage, the carbon capture rate is controlled with the reboiler steam valve. This allocation is summarized in Table 2.

Instead of using the solvent pump downstream the stripper to control the stripper temperature, the solvent pump downstream the absorber is often used to control the stripper temperature (Montanés et al., 2017). In this model, the control deviation during load changes is lower and the control is more robust when the solvent pump downstream the stripper is used to control the stripper temperature. The following case study focuses less on the load changing behavior of both control structures but on the capability of achieving a smooth change between

[1] Ramezan et al. recommend a maximum diameter of 12.2 m (40 ft)

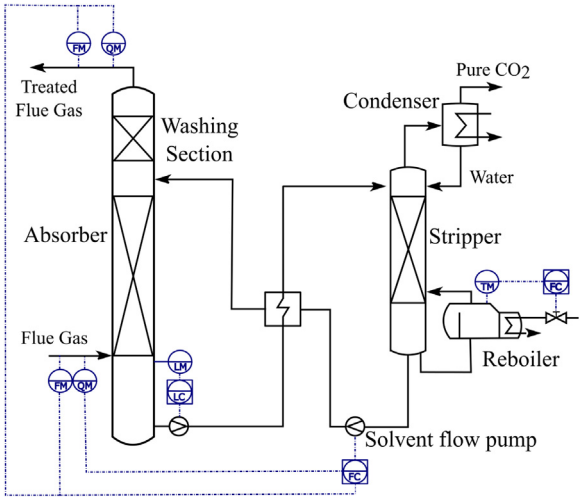

Fig. 4. Control structure A of pcc-plant.

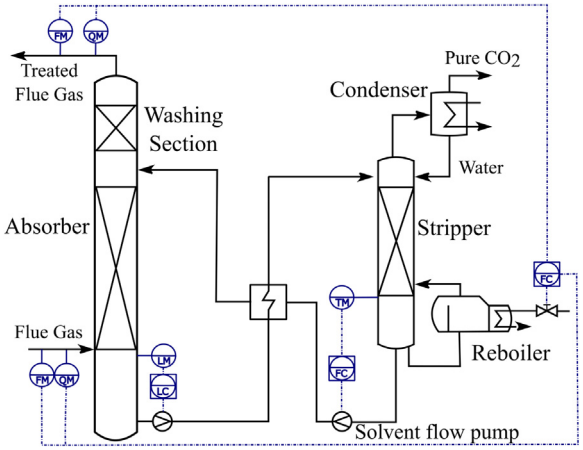

Fig. 5. Control structure B of pcc-plant.

Table 2
Overview of control structures.

Control	Manipulated variable	Control variable
A	$\dot{V}_L$	X_{CO_2}
	$\dot{Q}_{reb}$	T_{reb}
B	$\dot{V}_L$	$T_{str,1}$
	$\dot{Q}_{reb}$	X_{CO_2}

the start-up and regular operation.

As the process set points of the reboiler temperature and carbon capture rate cannot be controlled at the beginning of the start-up process, the controllers have to be operated in manual mode. For an automatic and safe start-up suitable switching conditions between the steps have to be found. One possible developed step sequence can be seen in Fig. 6. The effects and changes in these steps must ensure that the switching occurs in almost any event. For instance, when the solvent flow rate is too low compared to the power plant load, it could happen that the carbon capture rate of $X_{CO_2} = 90\%$ is not reached and the switching to the last step does not occur.

In the first step, the pcc-plant is in an empty state. Before the firing in the power plant is started, the solvent pumps have to be switched on to wet the columns and mix the solvent. When the firing in the power plant is started, the solvent flow rate should be set manually to an optimal L/G ratio (the ratio of solvent flow rate and flue gas flow rate). The optimal L/G ratio is dependent of the power plant load. This ensures that the solvent flow rate is sufficient to reach a carbon capture rate of $X_{CO_2} = 90\%$. A constant solvent flow rate is also possible but if the power plant load is increased comparatively fast after start-up, the solvent flow rate may not be sufficient for the target carbon capture rate. A higher constant solvent flow rate would lead to an inefficient pcc-plant operation at low partial loads. Therefore, the coupling of the solvent flow rate to the L/G-ratio is a good compromise. The constant solvent flow approach is tested in an alternative step sequence in a case study in the last section.

When the steam flow to the low pressure turbine is started and the pressure between the IP and LP turbine reaches 4 bar, the steam flow to the reboiler is started. In this case, a constant valve opening would be also possible but this could lead to the same problem as explained above in the case of the solvent flow rate. Nevertheless, this is also examined in the case study in the last section. In regular operation, approximately half of the steam mass flow to the low pressure turbine is used for the solvent regeneration. Hence, the steam flow to the reboiler is controlled in such a way that half of the steam flows into the reboiler. The gain and the reset time of the controller are adapted to perform this control task. After step 4, the controller parameters are reset to regular values. An additional benefit of this step is that the steam mass flow into the reboiler as well as the steam mass flow to the low pressure turbine cannot drop below a defined minimum value. As soon as a certain reboiler temperature (e.g. 120 °C) is reached, the temperature in the stripper or reboiler is controlled by the steam mass flow into the reboiler or the solvent flow rate depending on the control structure. When the carbon capture rate reaches its targeted value, the carbon capture rate is controlled by the remaining manipulated variable. In the model, the step sequence is parallelized after step 4 which means that step 6 can also be active before step 5 has been activated.

This step sequence shows the best performance with regard to stability. In the case study section, another possible step sequence is shown and the results are compared.

The alternative step sequence can be seen in Fig. 7. This step sequence can only be used with control structure A.

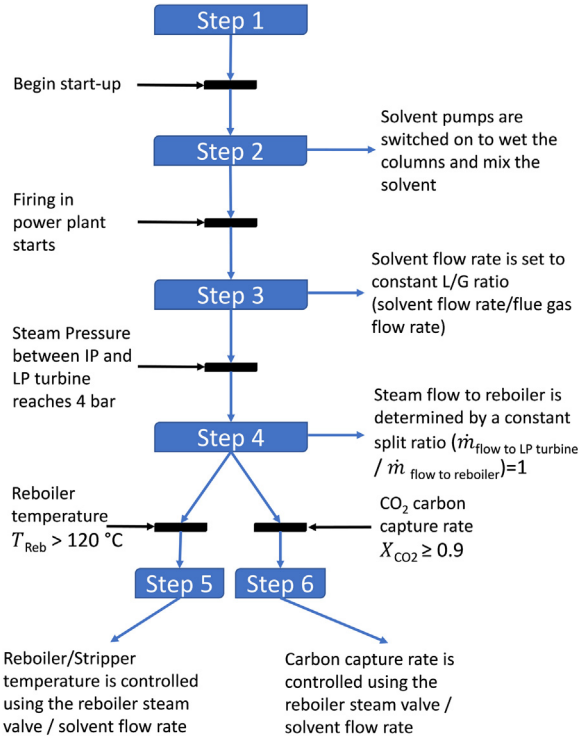

Fig. 6. Step sequence control structure.

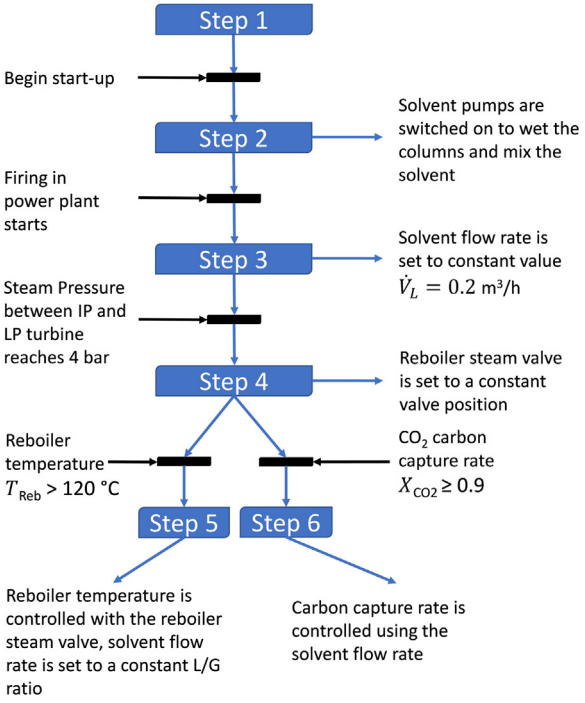

Fig. 7. Alternative step sequence control structure.

4. Simulation results

In this section, the simulation results of a reference hot start-up of the power plant with pcc-plant are shown. For the reference case, the load profile of a shutdown and a downtime of approximately 10 hours followed by a hot start-up is taken from a real start-up case of the power plant in Heyden. The control structure A (Fig. 4) and the reference step sequence (Fig. 6) are used for the simulation. The effect of the other control structure and step sequence are investigated in Section 5.4. The start-up is finished when the targeted capture rate within a relative tolerance of ± 3% is reached.

$$X_{CO_2,end} = 0.9 \pm 0.027 \quad (15)$$

The load profile that was used for the simulation is depicted in Fig. 8. It was taken from measurement results of the Heyden power plant.

In the reference scenario, the power plant is initialized at full load in steady state. After $t = 5000$ s the load is reduced with a constant load change rate of 1.57%/min. The load change rate is adjusted at $t = 7520$ s to 0.24%/min. After the load reduction, the plant is operated at a constant low partial load of 23% until the plant is shut down at $t = 15,600$ s. After a downtime of approximately 10 h, a hot start-up of the power plant is performed. The firing starts at $t = 50,000$ s. At $t = 51,000$ s, the air flow rate and the amount of fuel to the burner section is increased resulting in a higher heat output of the furnace. Subsequently, the produced steam is fed to the turbines and the pcc-plant. The power plant is again operated at a low partial load of 23% for a short time before the load of the power plant is increased to full load again.

In Fig. 9 the carbon capture rate during the simulation is shown. First, it is demonstrated that the pcc-plant can be operated at a constant carbon capture rate of $X_{CO_2} = 90\%$ also at low partial loads. When the power plant is shut down, the carbon capture rate drops to zero as the flue gas flow stops. Prior to the start of the firing, the solvent pumps in the pcc-plant are started. When the firing is started and the flue gas is fed to the absorption unit, the carbon capture rate increases to a high value of nearly 90% as the solvent is not saturated yet. As the solvent loading in the absorption unit increases and is not regenerated in the stripper yet, the carbon capture rate drops slowly to a lower value until the targeted temperature in the stripper is reached and the regeneration of the solvent starts. The capture rate increases slowly until the controller is switched on to control the carbon capture rate.

The oscillation in the carbon capture rate at $t = 51,000$ s occurs due to the fact that the air flow rate and the amount of fuel is increased resulting in a lower mass fraction of CO_2 in the flue gas at absorber inlet.

The start-up of the pcc-plant is started at $t = 46,000$ s, when the solvent pumps are switched on and all heat exchangers are put into operation. Using this defined start time, the calculated start-up time of the plant is 2.54 h.

Fig. 10 shows the reboiler temperature during shutdown, downtime and start-up operation. When the pcc-plant is shut down, the pressure in the stripper decreases. Therefore, the reboiler temperature drops to the boiling temperature of the solvent at ambient pressure and due to the heat loss to ambience the temperature continues to drop. When the solvent pumps are switched on at $t = 46,000$ s, the reboiler temperature decreases rapidly as the reboiler is cooled by the fresh solvent. After starting the steam supply, the reboiler temperature increases until the operation temperature is reached again.

The solvent flow rate is shown in Fig. 11. It decreases with decreasing power plant load to guarantee that the pcc-plant is operated at the optimal operating point. As the mass flow and CO_2 concentration of the flue gas flow decrease, the amount of solvent, that is needed for the absorption of the CO_2 in the flue gas, decreases. Therefore, the solvent flow rate corresponds to the power plant load.

The same applies to the graph of the steam flow rate behind the intermediate pressure turbine, which is split up into a part that is directed to the reboiler of the pcc-plant and a part that flows through the low pressure turbine, depicted in Fig. 12. Approximately half of the steam is needed for the regeneration of the solvent in the pcc-plant. After the power plant start-up, the steam mass flow is split up into two equal parts until the reboiler temperature is reached as presented in the step sequence in Fig. 6. When the reboiler temperature is reached, the steam flow to the pcc-plant is reduced slightly. Subsequently, the total steam flow continues to rise as the power plant load is increasing.

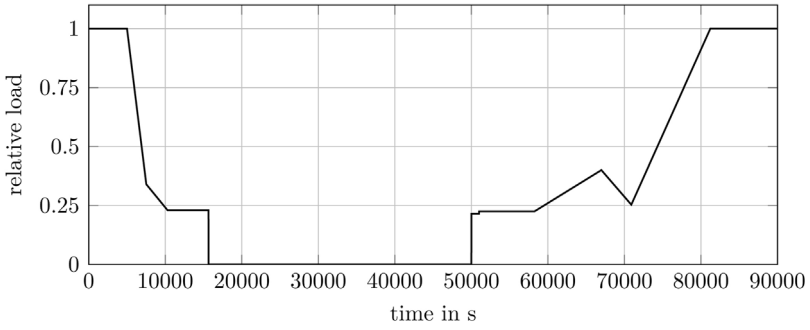

Fig. 8. Load profile of the simulated process used for the simulations.

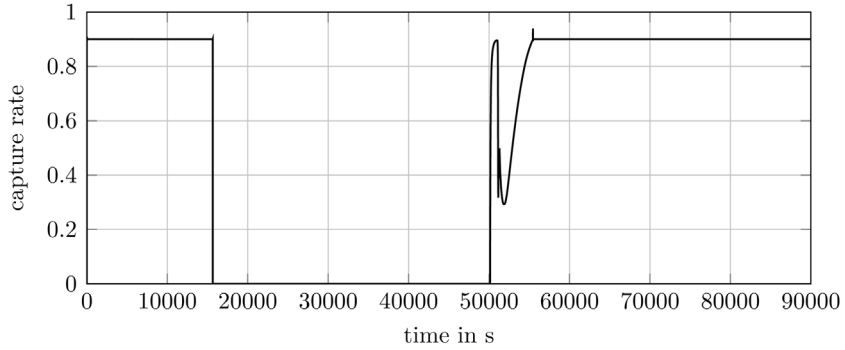

Fig. 9. Carbon capture rate during shutdown, downtime and start-up operation.

The solvent loading in the absorber and stripper sump are shown in Fig. 13. During normal operation, the rich and lean loading are only slightly changed as the reboiler temperature is controlled in such a way that the plant is operated at its optimal operation point. Before start-up, it is important that the solvent is mixed to get a homogeneous mixture. Therefore the solvent pumps are switched on one hour before power plant start. At the start-up time, the solvent loadings in the absorber and stripper reach the same value, which means that the solvent is mixed completely in the plant. During start-up, both solvent loadings increase until the regeneration of the solvent starts. Finally, the lean solvent loading decreases until a steady state value is reached.

The gross electric output of the power plant depicted in Fig. 14 is also related to the power plant load and shows nearly the same behavior

5. Case study

The previously outlined model is used for two different case studies. In the first case study, some input variables and parameters are changed and their influence on the start-up time are evaluated. In the second case study, the existing control system is compared with a different step sequence. Finally, their advantages and disadvantages are discussed.

All simulations of the first case study are carried out using Control Structure A and the step sequence control illustrated in Fig. 6.

5.1. Variation of different parameters

In this subsection, the influence of different parameters and process input variables is investigated. The solvent flow rate during start-up can be adjusted by the plant operator. Furthermore, the steam flow to the reboiler during start-up can also be varied if the limitation due to the power plant is taken into account. The variation of the total amount of solvent in the pcc-plant is also of interest as an increase of the total amount of solvent increases the stability of the plant but also increases start-up and settling times.

5.1.1. Variation of solvent flow rate

The solvent flow rate is adapted manually during start-up and is determined by the L/G ratio as depicted in the step sequence in Fig. 6. During start-up, this manual value can also be adapted in such a way that a faster start-up is achieved. To investigate the influence of the solvent flow rate on the start-up time, the solvent flow rate is varied by introducing a calibration factor k.

$$\dot{V}_{\mathrm{L}} = k \cdot \dot{V}_{\mathrm{L,opt}} \tag{16}$$

The start-up time for the reference scenario and both variations are shown in Table 3.

On the one hand, a reduction of the solvent flow rate leads to a significant increase of the start-up time as the carbon capture rate increases slower in this case. This can be explained by the reduced regeneration rate in the stripper sump. On the other hand, an increase of the solvent flow rate results in a decreasing start-up time as the regeneration rate in the stripper is increased and the targeted carbon capture rate is reached faster. In future optimization approaches, the model can be used to find the optimal calibration factor to minimize the start-up time.

It is also possible to use more complex step sequences. For instance, it would be possible to set a low solvent flow rate to increase the heat-up rate in the reboiler and to increase the solvent flow rate when the targeted reboiler temperature is reached. This can decrease the start-up time even more as shown in a previous publication (Marx-Schubach and Schmitz, 2017).

However, the optimal constant solvent flow rate or optimal solvent flow rate trajectory is dependent on many different specific plant characteristics and a general recommendation for all pcc-plants cannot be given.

5.1.2. Variation of steam flow rate

In a similar way, the steam flow rate to the reboiler is varied. To vary the steam flow rate, the controller nominal value of the ratio between the steam mass flow to the reboiler and the steam mass flow to

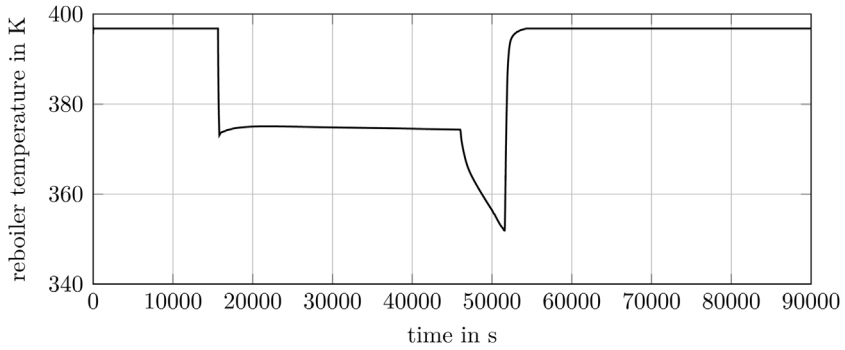

Fig. 10. Reboiler temperature in K during shutdown, downtime and start-up operation.

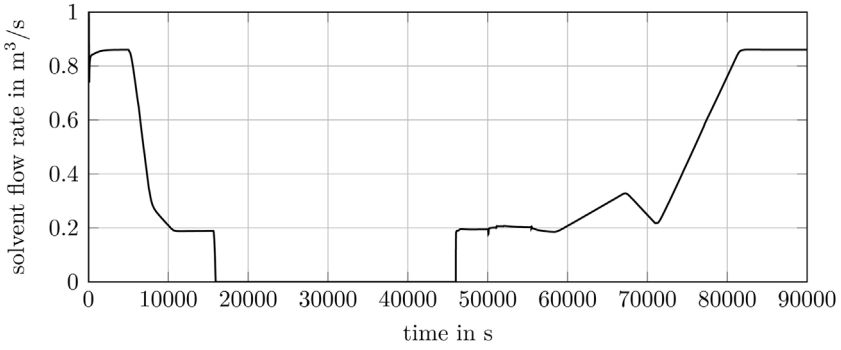

Fig. 11. Solvent flow rate in m^3/s during shutdown, downtime and start-up operation.

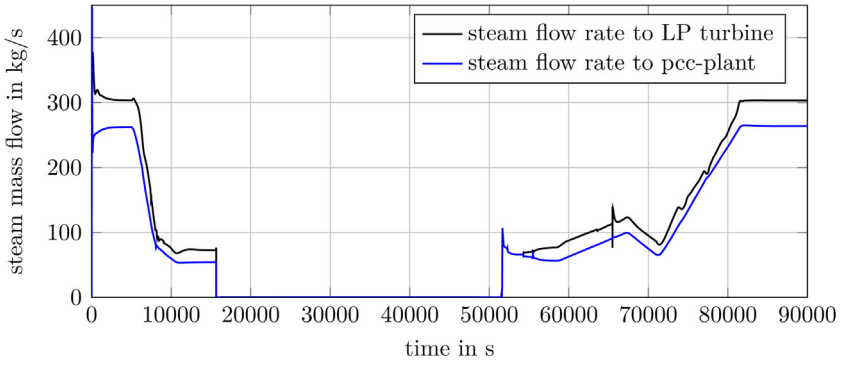

Fig. 12. Steam flow rate during shutdown, downtime and start-up operation.

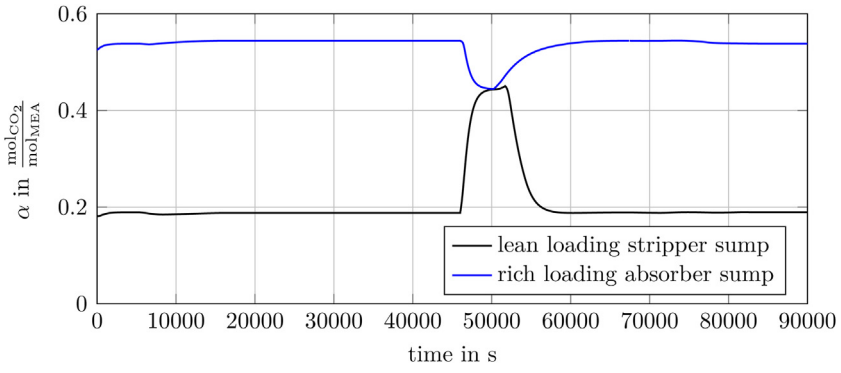

Fig. 13. Solvent loading during shutdown, downtime and start-up operation.

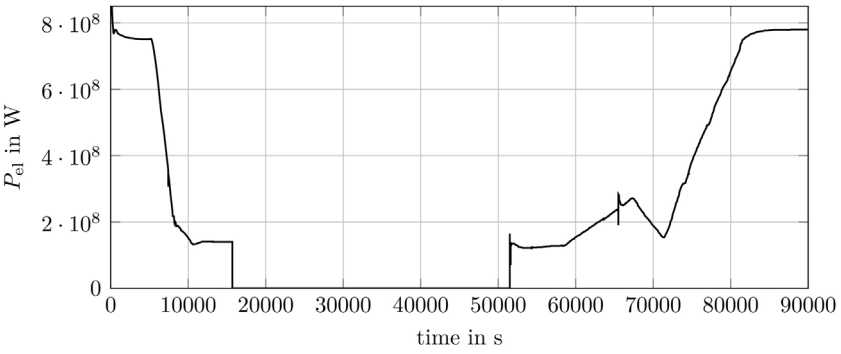

Fig. 14. Gross electric output of the power plant during shutdown, downtime and start-up operation.

the LP turbine is changed. In the reference scenario a factor of 1 was used.

$$\frac{\dot{m}_{\text{steam,Reb}}}{\dot{m}_{\text{steam,LP}}} = k \tag{17}$$

The start-up time for the reference scenario and both variations are shown in Table 4 .

Table 3
Comparison of start-up time when varying the solvent flow circulation rate.

Variable	Ref.	$k = 0.9$	$k = 1.1$
Start-up time in h	2.54	3.14	2.46

Table 4
Comparison of start-up time when varying the steam flow rate into the reboiler.

Variable	Ref.	$k = 0.9$	$k = 1.1$
Start-up time in h	2.54	2.64	2.48

Table 5
Comparison of start-up time when varying the total amount of solvent.

Variable	Ref.	−30%	+30%
Start-up time in h	2.54	2.32	2.67

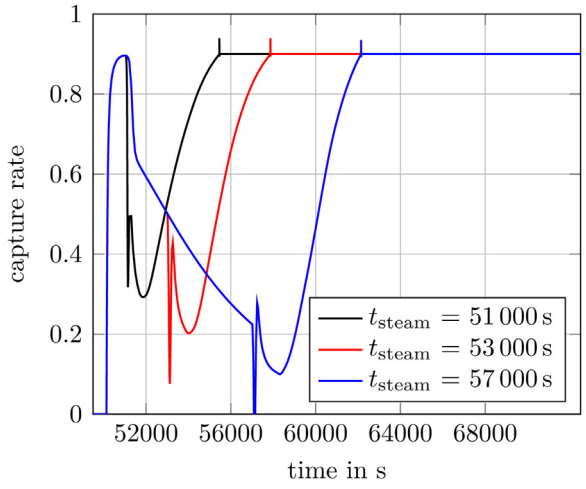

Fig. 15. Carbon capture rate results when varying steam supply time.

Table 6
Comparison of start-up time when varying the total amount of solvent.

Variable	Ref.	$t_{st.} = 53,000$ s	$t_{st.} = 57,000$ s
Total start-up time in h	2.54	3.20	4.42
Start-up time after steam supply in h	1.15	1.25	1.36

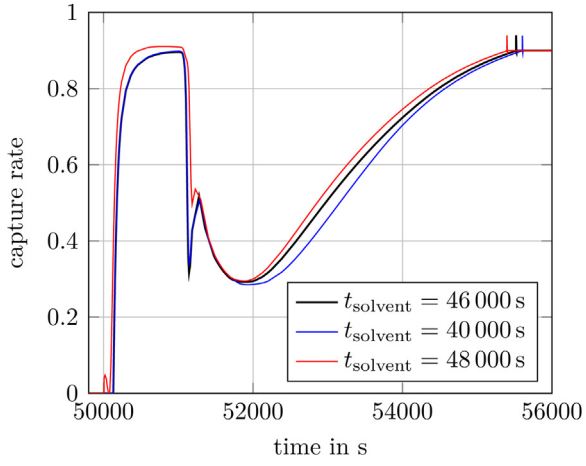

Fig. 16. Carbon capture rate during start-up.

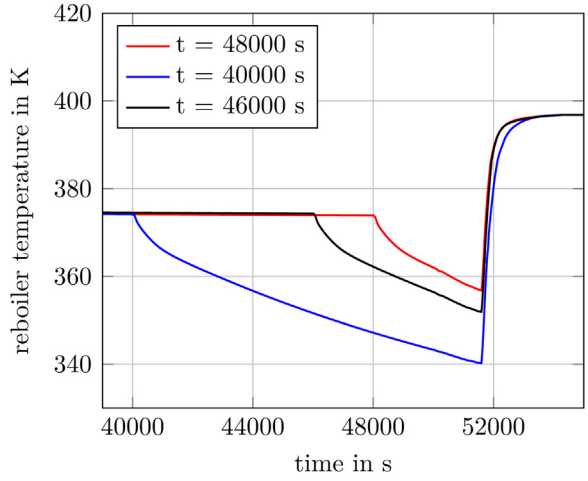

Fig. 17. Reboiler temperature in K during shutdown, downtime and start-up operation.

Table 7
Comparison of start-up time when varying the start of the solvent flow rate.

Variable	Ref.	$t_{solvent} = 40,000$ s	$t_{solvent} = 48,000$ s
Total start-up time in h	2.54	2.57	2.51

As expected, the start-up time decreases when the steam flow rate is increased. It is worth mentioning, a reduction of the steam flow leads to a larger absolute change in start-up time then an increase of the steam flow rate.

5.1.3. Variation of total amount of solvent

The total amount of solvent in the pcc-plant in the reference scenario is 1107 m^3. The total amount of solvent is increased and decreased by 30% in the stripper and absorption sump in this case study.

The start-up time for the reference scenario and the variations are shown in Table 5.

The start-up time increases with increasing total amount of solvent as more solvent has to be heated up and regenerated.

5.2. Variation of steam supply time

In this subsection, the steam supply time to the reboiler is varied. The firing of the power plant starts at $t = 50,000$ s. At $t = 51,000$ s the fuel and air input into the combustion chamber is increased to put the steam generator in operation. Subsequently, the produced steam flows through the turbines and the reboiler valve is opened to heat up the solvent. The time between those two events is increased in this case study, leading to a longer total start-up time. The results of the carbon capture rate are shown in Fig. 15. The solvent flow rate pumps are switched on at $t = 46,000$ s in all three cases and the reboiler temperature is decreasing until the steam to the reboiler is supplied. Therefore, also the start-up time after steam supply increases, when the steam supply time is delayed. The slope of the carbon capture rate is lower in the delayed cases. The results of both start-up times are outlined in Table 6.

5.3. Variation of the start-up time of solvent pumps

The solvent pumps must be switched on to fill the columns before the flue gas enters the absorption unit. Furthermore, the solvent pumps are used to mix the solvent and to prevent an uneven composition of the solvent. In the following, the influence of the start-up time of the solvent pumps will be investigated.

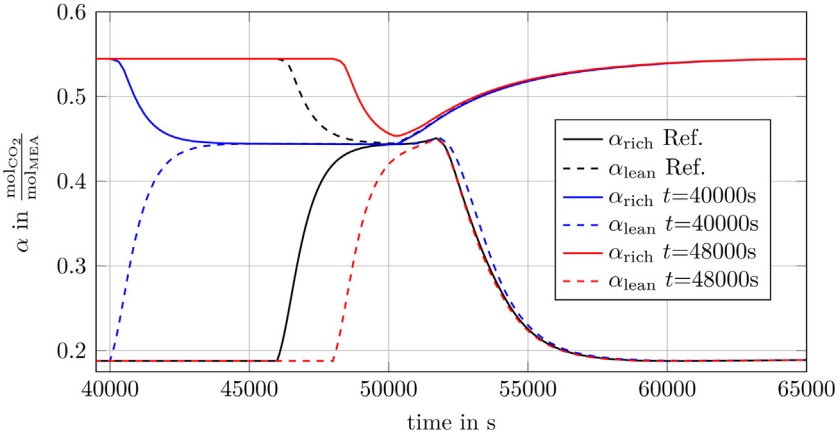

Fig. 18. Rich and lean loading in the carbon capture plant during start-up.

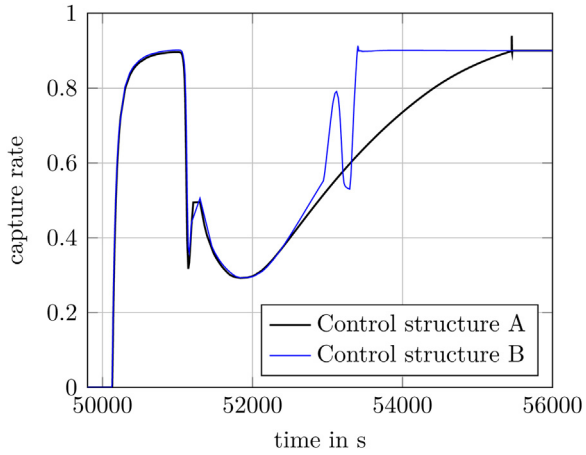

Fig. 19. Comparison of two control structures: carbon capture rate.

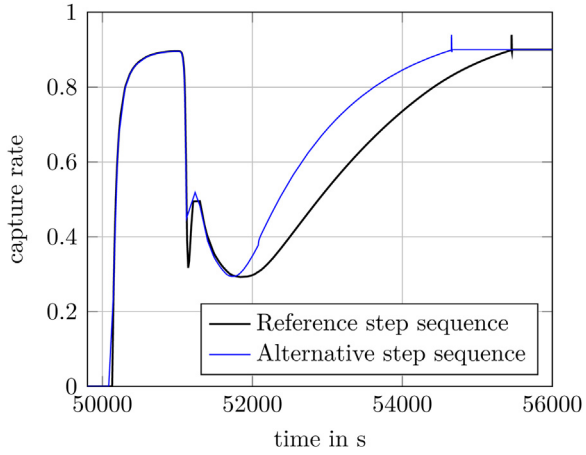

Fig. 20. Comparison of two sequential step sequences: carbon capture rate.

In Fig. 16 the carbon capture rate of the reference case and two other cases are compared. In one case, the start of the solvent flow rate is delayed and in the other case, the solvent flow rate pumps are switched on earlier. As expected, the start-up time decreases when the solvent flow rate pumps are started later.

The reason can be seen in Fig. 17. The reboiler temperature decreases due to the circulation of the fresh solvent in the plant. As a result, the steam supply starts at a lower reboiler temperature resulting in a longer start-up time. The start-up times are compared in Table 7.

To minimize the start-up time, the solvent flow rate pumps should be switched on as late as possible. However, this effect on the start-up time is comparatively low in the time period from $t_{solvent}$ = 40, 000 s until $t_{solvent}$ = 48, 000 s. To examine the mixing process of the solvent, the rich and lean solvent loading in the absorber and stripper sump of all three cases are illustrated in Fig. 18. It can be concluded that the start of the solvent flow rate pumps at $t_{solvent}$ = 46, 000 s is just sufficient to achieve a complete mixing of the solvent. When the solvent flow rate pumps are started at $t_{solvent}$ = 48, 000 s the solvent is not mixed completely as the rich and lean loading are not the same at time instant $t_{solvent}$ = 50, 000 s. It can be summarized that approximately one hour of solvent mixing time is needed with a total amount of solvent of 1107 m^3.

5.4. Variation of pcc-plant control structures

In the last case study different control structures and sequential control structures are compared. In Section 3.4 two control structures from the literature are presented. Furthermore, two different sequential control sequences are developed and presented.

In a first step, the reference step sequence depicted in Fig. 6 is used for the simulation and the control structure is changed from control structure A to control structure B. The resulting carbon capture rate during start-up is shown in Fig. 19 for both control structure.

At the beginning of the start-up, the carbon capture rates show the same behavior in both cases until the targeted reboiler temperature is reached. In the reference case (control structure A) the reboiler temperature is controlled by the steam pressure valve at the steam inlet. When the desired reboiler temperature is reached, the steam valve is throttled slightly which can be seen in Fig. 12. As the impact of the reboiler steam valve on the capture rate only takes effect with a long delay, the carbon capture rate shows no fluctuations at this point. In the second case (control structure B), the stripper temperature is controlled by the solvent flow rate pump downstream the stripper. By the time the targeted temperature is reached, the controller is switched on. The solvent flow rate is increased to control the stripper temperature as the steam flow to the reboiler is slightly higher than needed. The dead time of the carbon capture rate, when the solvent flow rate is changed, is much lower than in the reference case. Therefore, a significant fluctuation can be seen in the carbon capture rate.

The carbon capture rate reaches its target value much faster than with control structure A. This can be explained by two reasons. First, the mean steam flow to the reboiler during start-up is higher when using control structure B as the steam flow is not reduced until the carbon capture rate of 90% is reached. Second, the controller increases the solvent flow rate to control the reboiler temperature resulting in a faster decrease of the solvent loading in the stripper sump. Increasing the solvent flow rate, after the reboiler reached its operation

temperature, results in a decreasing start-up time as shown in an earlier publication (Marx-Schubach and Schmitz, 2017).

It can be outlined that the control structure B results in a faster start-up time but also increases the fluctuations of the carbon capture rate which could lead to stability issues in the pcc-plant. It also should be noted that the choice of the control structure in regular operation has also a high impact on the start-up process.

In addition to varying the control structure, it is also possible to choose another step sequence. In the alternative step sequence (Fig. 7), the focus is on choosing constant values for the manual operation mode of the controllers. The resulting carbon capture rate is illustrated in Fig. 20. For these simulations, control structure A was used.

In this case, the start-up time of the alternative step sequence is shorter than in the reference case. The start-up time depends on the constant value of the reboiler steam valve opening. Here, the steam flow to the reboiler is higher than in then reference case. If a lower value for the constant valve opening was chosen, the result was a higher start-up time. However, for much lower valve opening values stability problems could be observed, as the steam flow to the reboiler was not sufficient to reach the targeted reboiler temperature especially when small disturbances occur. Although this step sequence results in a lower start-up time, the stability of this step sequence is lower compared to the reference sequence. Small disturbances in a lot of process variables, for example the pressure in the water steam cycle, could result in an unstable start-up making manual interventions necessary.

Beyond these step sequence controllers also other step sequences are a possible option. Instead of controlling the ratio between the steam mass flows to the reboiler and the low pressure turbine, one could also control the power generation during start-up using the reboiler steam valve if required.

6. Conclusion and outlook

In this contribution, the development of a simplified power plant model and a more detailed pcc-plant model is shown. The model is capable of simulating the start-up and shutdown process, as well as the regular operation in a load range of 23–100% of the combined process. The model is used to develop appropriate control structures and step sequences for the pcc-plant to allow an automatic start-up of the combined process.

The results indicate that the total start-up time of the pcc-plant when performing a hot start simultaneously with the power plant is 2.54 h in the reference case. The case study shows that a variation of the solvent flow rate has a high impact on the start-up time. It can be concluded that the choice of the correct solvent flow rate trajectory is essential for a fast and stable start-up. As expected, a higher steam flow rate to the reboiler results in a decreased start-up time and a higher total amount of solvent in an increased start-up time. Additional case studies point out that the choice of an appropriate control structure and a suitable step sequence are important for the start-up of the combined process in order to minimize the start-up time or to increase the stability of the plant.

Further studies should focus on the impact of the pcc-plant on the power plant during start-up in more detail. For this purpose, a more detailed power plant model is desirable to study the restrictions, effects and limitations imposed by the pcc-plant. Additionally, the control structures of the power plant and pcc-plant should be extended to develop a more detailed control system. In a real case scenario, the developed model could be used to optimize the start-up process with regard to the start-up time or energy demand.

Acknowledgement

This research project has been supported by the German Federal Ministry for Economic Affairs and Energy (project number 03ET7060B) which is greatly acknowledged.

Furthermore, the model of the power plant was provided by the Institute of Energy Systems at the Hamburg University Technology. The provision of the model is greatly acknowledged.

References

Agbonghae, E.O., Hughes, K.J., Ingham, D.B., Ma, L., Pourkashanian, M., 2014. Optimal process design of commercial-scale amine-based CO_2 capture plants. Ind. Eng. Chem. Res. 53 (38), 14815–14829.

Åkesson, J., Laird, C.D., Lavedan, G., Prölß, K., Tummescheit, H., Velut, S., Zhu, Y., 2012. Nonlinear model predictive control of a CO_2 post-combustion absorption unit. Chem. Eng. Technol. 35 (3), 445–454.

Bhown, A.S., Freeman, B.C., 2011. Analysis and status of post-combustion carbon dioxide capture technologies. Environ. Sci. Technol. 45 (20), 8624–8632.

Bui, M., Gunawan, I., Verheyen, V., Feron, P., Meuleman, E., Adeloju, S., 2014. Dynamic modelling and optimisation of flexible operation in post-combustion CO_2 capture plants – a review. Comput. Chem. Eng. 61, 245–265.

ClaRa-Library, 2019. ClaRa – Simulation of Clausius-Rankine cycles. URL http://www.claralib.com.

Cooke, David H., 1984. On prediction of off-design multistage turbine pressures by Stodola's ellipse. 1984 Joint Power Generation Conference: GT Papers.

Dietl, K., 2012. Equation-Based Object-Oriented Modelling of Dynamic Absorption and Rectification Processes. Hamburg University of Technology, Hamburg Ph.D. Thesis.

Dutta, R., Nord, L.O., Bolland, O., 2017. Selection and design of post-combustion CO_2 capture process for 600 MW natural gas fueled thermal power plant based on operability. Energy 121, 643–656.

Alobaid, Falah, 2018. Numerical Simulation for Next Generation Thermal Power Plants. Springer International Publishing AG, Cham, Switzerland.

Gottelt, Friedrich, Hoppe, Timm, Nielsen, Lasse, 2017. Applying the Power Plant Library ClaRa for Control Optimisation. 12th Modelica Conference Proceedings. Linköping Electronic Conference Proceedings 867–877 Linköping University Electronic Press.

Garðarsdóttir, S.Ó., Montanés, R.M., Normann, F., Nord, L.O., Johnsson, F., 2017. Effects of CO_2 – absorption control strategies on the dynamic performance of a supercritical pulverized-coal-fired power plant. Ind. Eng. Chem. Res. 56 (15), 4415–4430.

Gaspar, J., Jorgensen, J.B., Fosbol, P.L., 2015. Control of a post-combustion CO_2 capture plant during process start-up and load variations. IFAC-PapersOnLine 48 (8), 580–585.

Jayarathna, S.A., Lie, B., Melaaen, M.C., 2013. Dynamic modelling of the absorber of a post-combustion CO_2 capture plant: modelling and simulations. Comput. Chem. Eng. 53, 178–189.

Joos, A., Dietl, K., Schmitz, G., 2009. Thermal separation: an approach for a Modelica Library for absorption, adsorption and rectification. In: Modelica Asscociation (Ed.), 7th Modelica Conference Proceedings. Linköping Electronic Conference Proceedings. Linköping University Electronic Press, pp. 804–813.

Kister, H.Z., 1992. Distillation Design. McGraw Hill, New York.

Kvamsdal, H.M., Jakobsen, J.P., Hoff, K.A., 2009. Dynamic modeling and simulation of a CO_2 absorber column for post-combustion CO_2 capture. Chem. Eng. Process.: Process Intensif. 48 (1), 135–144.

Lawal, A., Wang, M., Stephenson, P., Obi, O., 2012. Demonstrating full-scale post-combustion CO_2 capture for coal-fired power plants through dynamic modelling and simulation. Fuel 101, 115–128.

Leung, D.Y., Caramanna, G., Maroto-Valer, M.M., 2014. An overview of current status of carbon dioxide capture and storage technologies. Renew. Sustain. Energy Rev. 39, 426–443.

Lew, D., Brinkman, G., Kumar, N., Besuner, P., Agan, D., Lefton, S., 2012. Impacts of Wind and Solar on Fossil-Fueled Generators. IEEE Power and Energy Society General Meeting, San Diego, CA.

Lin, Y.-J., Wong, D.S.-H., Jang, S.-S., Ou, J.-J., 2012. Control strategies for flexible operation of power plant with CO_2 capture plant. AIChE J. 58 (9), 2697–2704.

Luu, M.T., Abdul Manaf, N., Abbas, A., 2015. Dynamic modelling and control strategies for flexible operation of amine-based post-combustion CO_2 capture systems. Int. J. Greenhouse Gas Control 39, 377–389.

Mac Dowell, N., Shah, N., 2014. Dynamic modelling and analysis of a coal-fired power plant integrated with a novel split-flow configuration post-combustion CO_2 capture process. Int. J. Greenhouse Gas Control 27, 103–119.

Mac Dowell, N., Shah, N., 2015. The multi-period optimisation of an amine-based CO_2 capture process integrated with a super-critical coal-fired power station for flexible operation. Comput. Chem. Eng. 74, 169–183.

Marx-Schubach, T., Schmitz, G., 2017. Optimizing the start-up process of post-combustion capture plants by varying the solvent flow rate. 12th Modelica Conference Proceedings. Linköping Electronic Conference Proceedings 121–130 Linköping University Electronic Press.

Marx-Schubach, T., Schmitz, G., 2018. Dynamic simulation and investigation of the startup process of a postcombustion-capture plant. Ind. Eng. Chem. Res. 57 (49), 16751–16762.

Mechleri, E., Lawal, A., Ramos, A., Davison, J., Dowell, N.M., 2017. Process control strategies for flexible operation of post-combustion CO_2 capture plants. Int. J. Greenhouse Gas Control 57, 14–25.

Mejdell, T., Haugen, G., Rieder, A., Kvamsdal, H.M., 2017. Dynamic and control of an absorber – desorber plant at Heilbronn. Energy Procedia 114, 1231–1244.

Modelica Association, 2017. Modelica – A Unified Object-Oriented Language for Systems Modeling, Version 3.4. URL https://www.modelica.org/documents/ModelicaSpec34.pdf.

Montanés, R., Flø, N., Nord, L., 2017. Dynamic process model validation and control of

the amine plant at CO_2 Technology Centre Mongstad. Energies 10 (10), 1527.
Montanés, R.M., Flø, N.E., Nord, L.O., 2018. Experimental results of transient testing at the amine plant at Technology Centre Mongstad: open-loop responses and performance of decentralized control structures for load changes. Int. J. Greenhouse Gas Control 73, 42–59.
Montanés, R.M., Garðarsdóttir, S.Ó., Normann, F., Johnsson, F., Nord, L.O., 2017b. Demonstrating load-change transient performance of a commercial-scale natural gas combined cycle power plant with post-combustion CO_2 capture. Int. J. Greenhouse Gas Control 63, 158–174.
Nittaya, T., Douglas, P.L., Croiset, E., Ricardez-Sandoval, L.A., 2014. Dynamic modelling and control of MEA absorption processes for CO_2 capture from power plants. Fuel 116, 672–691.
Oexmann, J., 2011. Post-combustion CO_2 capture: energetic evaluation of chemical absorption processes in coal-fired steam power plants. Hamburg University of Technology, Hamburg Ph.D. thesis.
Panahi, M., Skogestad, S., 2011. Economically efficient operation of CO_2 capturing process. Part I: Self-optimizing procedure for selecting the best controlled variables. Chem. Eng. Process.: Process Intensif. 50 (3), 247–253.
Panahi, M., Skogestad, S., 2012. Economically efficient operation of CO_2 capturing process. Part II. Design of control layer. Chem. Eng. Process.: Process Intensif. 52, 112–124.
Ramezan, M., Skone, T.J., Nsakala ya Nsakala, Liljedahl, G.N., 2007. Carbon Dioxide Capture from Existing Coal-Fired Power Plants – Final Report. National Energy Technology Laboratory (NETL).
Rieder, A., Unterberger, S., 2013. EnBW's post-combustion capture pilot plant at Heilbronn – results of the first year's testing programme. Energy Procedia 37, 6464–6472.
Rochelle, G.T., 2009. Amine scrubbing for CO_2 capture. Science (New York, NY) 325 (5948), 1652–1654.
Sepideh Ziaii Fashami, 2012. Dynamic Modeling, Optimization, and Control of Monoethanolamine Scrubbing for CO_2 Capture. The University of Texas at Austin PhD Thesis.
Sulzer Chemtech, 2018. Structured Packings for Distillation, Absorption and Reactive Distillation. URL https://www.sulzer.com/-/media/files/products/separation-technology/distillation-and-absorption/brochures/structured_packings.ashx.
Szodrai, F., Lakatos, A., 2014. Measurements of the thermal conductivities of some commonly used insulating materials after wetting. Environ. Eng. Manage. J. 13 (11), 2881–2886.
VDI e.V, 2013. VDI-Wärmeatlas, 11th edition. Springer Vieweg, Berlin.
Walters, M.S., Edgar, T.F., Rochelle, G.T., 2016. Regulatory control of amine scrubbing for CO_2 capture from power plants. Ind. Eng. Chem. Res. 55 (16), 4646–4657.
Wang, L., Li, P., Wozny, G., Wang, S., 2003. A startup model for simulation of batch distillation starting from a cold state. Comput. Chem. Eng. 27 (10), 1485–1497.
Wellner, K., Marx-Schubach, T., Schmitz, G., 2016. Dynamic behavior of coal-fired power plants with postcombustion CO_2 capture. Ind. Eng. Chem. Res. 55 (46), 12038–12045.
Wellner, K.C., 2016. Simulation des dynamischen Verhaltens von thermischen Trennprozessen am Beispiel der CO_2-Abtrennung [Simulation of the dynamic behaviour of thermal separaration processes using the carbon capture process as an example] (in German). Hamburg University of Technology, Hamburg PhD Thesis.
Wu, X., Shen, J., Li, Y., Wang, M., Lawal, A., 2018. Flexible operation of post-combustion solvent-based carbon capture for coal-fired power plants using multi-model predictive control. A simulation study. Fuel 220, 931–941.
Zhang, Q., Turton, R., Bhattacharyya, D., 2016. Development of model and model-predictive control of an MEA-based postcombustion CO_2 capture process. Ind. Eng. Chem. Res. 55 (5), 1292–1308.